Numerical assessment of effects of dimension and layup on a bonded composite section joint design

Gang Li*, Chun Li, John Naftel

Aerospace Research Centre
National Research Council Canada, 1200 Montreal Road, Ottawa, ON, Canada K1A 0R6

Abstract

Design assessment of a bonded composite section joint was conducted using three-dimensional finite element (FE) methods via Nastran code in version 2015r1. Linear conventional shell elements were used in the numerical models. The joint consisted of a 3D "hat" shaped stiffener and a flat panel, in which the stiffener was thicker than the panel. The joint strength was controlled by the bond strength or the panel capability at the inner overlap end. Typically, a high stress ratio, panel/stiffener, was created at the inner overlap end. The high stress ratio was preferred in the design selection, which ensured the initial damage onset and subsequent failure occurrence at this prescribed location. Variation of the peak von Mises stress ratio was investigated under influences of the joint dimension, composite layup, and displacement boundary condition. Recommendations for the joint design were then proposed accordingly. Further, prediction of the joint static failure force and failure behaviour was carried out using an advanced FE model with continuum shell elements via Abaqus/CAE code in version 6.14r2. Cohesive behaviour technique with proper damage law and damage evolution model was employed to control the interface performance between the stiffener and the panel at the bonded section, in which the actual adhesive layer was not included in the model. With the predicted joint failure force, joint steel fixtures were properly fabricated that made the joint test completed successfully. Good agreement in the joint static failure force and progressive failure behaviour was obtained between the experimental and numerical results; the difference between the predicted and experimentally measured failure force was less than 1% magnitude.

***Keywords**: Bonded composite section joint; Design; Failure; Finite element; Static strength.*

1. Introduction

Fibre reinforced composite primary and secondary aircraft structures have the potential to achieve the same strength and stiffness as conventional metallic structures. Quasi-isotropic laminated composite panels are usually used in aerospace applications, since these types of layups are able to maintain satisfactory strength in both longitudinal and hoop directions. With considerable achievements in adhesive and bonding technologies, bonded composite structures can be lighter

* Corresponding author, Tel. (613) 990-4989, Fax: (613) 998-8609, E-mail: Gang.Li@nrc-cnrc.gc.ca.

and more cost-effective than equivalent bolted or riveted ones [1, 2]. Bonded composite structures have high potential for more applications in advanced aerospace vehicles [2-4].

This report presents a three-dimensional (3D) finite element (FE) study assessing (i) a bonded composite section joint design and (ii) the failure load of the designed joint. The joint design proposal was carried out simulating a tail boom joint configuration of the CH-149 Cormorant helicopter used by the Royal Canadian Air Force (RCAF). The location and configuration of this aircraft tail boom joint are shown in Fig. 1. A total of four tail boom joints, each located at a corner position, are used in the CH-149 tail boom section. The joint consists of a monolithic carbon-fiber reinforced stiffener which is bonded and bolted to a composite sandwich panel. It carries a mixed load condition of tension in the joint longitudinal direction and shear at the stiffener-panel overlap section. Within the constraints of the research objective and available resources in terms of budget, laboratory condition, material quantity and availability, and research schedule, a monolithic laminate panel, a constant cross-section stiffener, and bonded attachment method were adopted in the current joint design. These simplifications did not change the major loading feature as identified from the actual joint. Fig. 2 shows the joint design configuration that consisted of a 3D "hat" shaped stiffener and a flat panel made from carbon/epoxy prepregs or tapes. The joint strength should be dominated by the bond strength or the composite panel condition at the inner bonded end [1, 5, 11-13]. The joint design assessment was carried out using Nastran code in version 2015r1. The effects of dimension and composite layup on peak stress ratio, panel/stiffener, at the inner overlap end were studied using the FE models with conventional shell elements. Based on the variation of the peak stress ratio, design recommendations were proposed. Further, an advanced 3D FE model using continuum shell element was developed via Abaqus/CAE code in version 6.14r2 to predict the failure load of the designed joint. The surface-based cohesive behaviour technique was used to control the panel/stiffener interface interaction property [14-21]. Geometrically nonlinear behaviour was set in the model analysis. Using the predicted failure load, steel test fixtures were appropriately designed and fabricated to ensure joint test success. The numerical work greatly improved the experimental work progression in the joint design and fixture strength consideration.

The objectives of the work were to: (1) enrich the existing numerical modelling expertise to improve design and analysis of complex shaped bonded composite joints, (ii) emphasize the importance of application numerical modelling methods to support engineering design and analysis, and (iii) support further numerical analysis of bonded composite joint performance under representative influence factors such as environmental degradation and specific damage conditions.

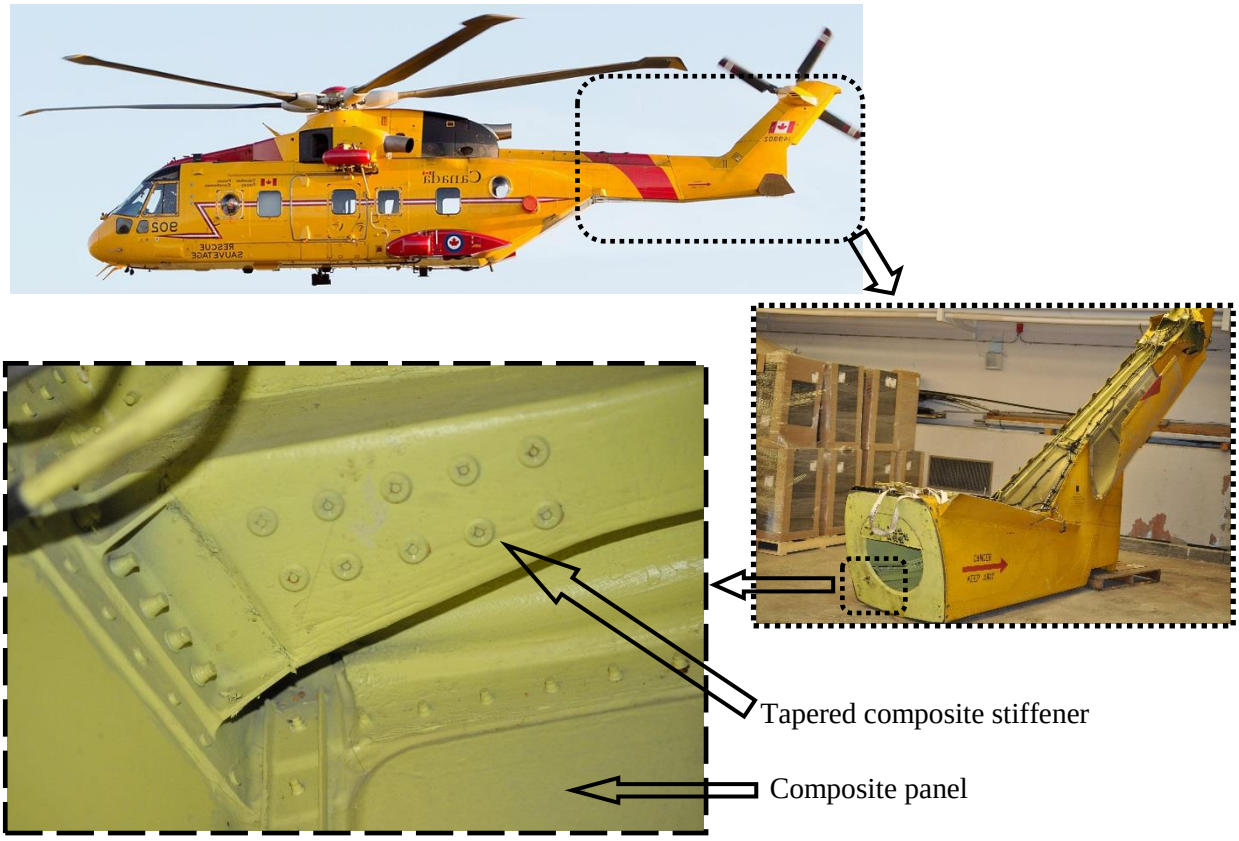

Fig. 1. Schematic images showing: (a) a CH-149 Cormorant helicopter with four joints in the aircraft tail boom section, and (b) the tail boom joint location and joint configuration.

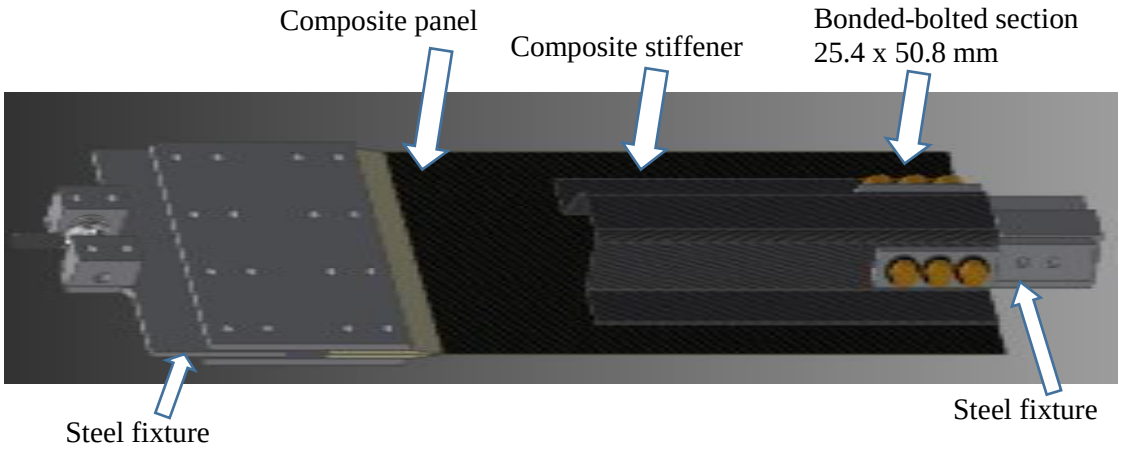

Fig. 2. The designed composite joint structure with steel end fixtures.

2. Materials and design assessment

2.1.Materials

The composite joint was to be made with high profile carbon fibre-reinforced composites. The composite material should be similar to the material supplied by Cytec Engineered Materials, such as the CYCOM-5276-1 carbon/epoxy G40-800 tapes with 0.127 mm thick tape/lamina. Film adhesive AF163-2K, which has a knit carrier, was used to bond the composite joint and the adhesive layer thickness was controlled to be 0.15 mm. The material mechanical parameters are given in Table 1.

Table 1. Material parameters for the bonded laminated composite joint [17, 18].

Laminar/Tape	Parameters at RT condition	Source
Modulus	E_{11}= 155GPa, E_{22} = 8.9GPa, G_{12} = G_{13} = 4.8GPa, G_{23} = 2.5GPa, and ν_{12} = 0.31	Technical datasheet of CYCOM 5276-1 toughened epoxy resign
Film adhesive AF163-2K-knit supported	Bulk parameter: E_a= 1.1GPa, G_a = 0.41GPa, and ν_a = 0.34	Technical datasheet (November 2009) of 3M Scotch-Weld™ Structural Adhesive Film AF 163-2

2.2.Design factors and assessment strategy

2.2.1 Design factors

Two factors were considered for the joint design; one was the joint dimension and the other was the laminate layup condition.

Dimensional variables

The schematic diagram of the joint in tension is shown in Fig. 3, where Fig. 3(a) is a side view showing the tensile loading condition and the highly stressed location at the inner bonded overlap end, Fig. 3(b) is a top view, and Fig. 3(c) is the cross-section of the bonded joint section. Three dimensions, L0, L3, and W3 were not included in the numerical design assessment. The L0 long tabbed panel edge section was replaced by an appropriate displacement boundary condition in the numerical models. The stiffener/fixture bonded-bolted section, in 25.4 x 50.8 mm section, was used to apply tensile load. W3 was a fixed dimension between the two inner the stiffener risers at the bottom side due to a fixed dimension of the stiffener used. Therefore, only four dimensional variables, L1, L2, W1, and W2, were assessed for the joint size determination. In which: (i) L1 was the unbonded panel section length between the inner bonded overlap end to the tabbed inner edge; (ii) L2 was the stiffener length that was also the bonded section length; (iii) W1 was the

unbonded panel width outside the bonded section; and (iv) W2 was the bonded width between the stiffener and the panel.

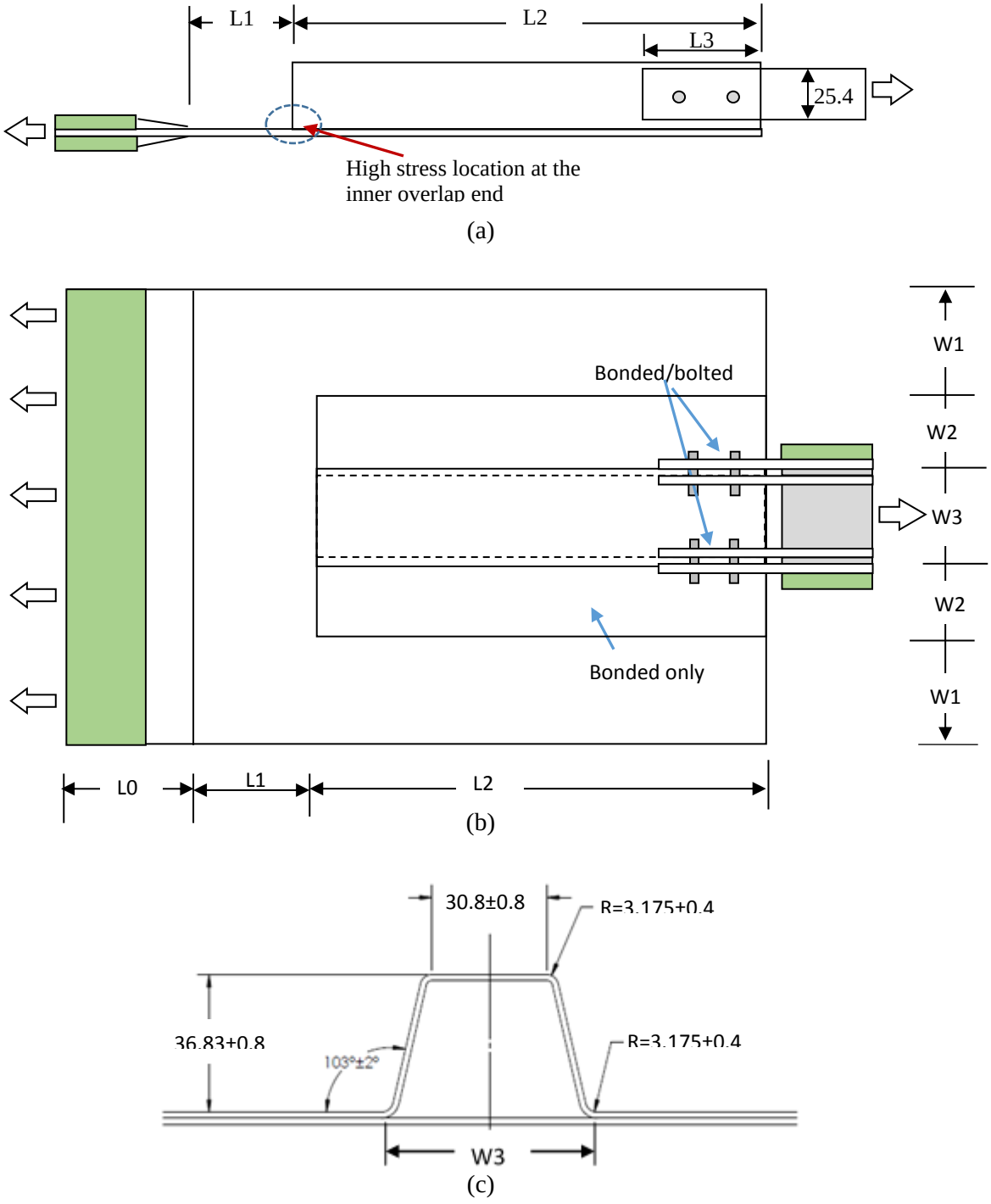

Fig. 3. Schematic diagrams with the dimensional variables used in the numerical assessment for the joint design with a constant cross-section stiffener, where (a) shows the side view, (b) shows the top view, and (c) shows the fixed cross-section of the stiffener used to bond the panel (dimensions: mm).

Layup consideration

Typically, balanced and symmetric layups are used in laminated composite structures to ensure sufficient strength in all directions within its plane. Considering actual loading conditions, extra plies are usually added to the laminated composite structures to ensure enough strength in specific directions. However, balanced and symmetric layup conditions are still kept. This layup condition can effectively limit possible warpage and hence considerably reduce stress concentration [11-13], which was adopted in the current joint design consideration. After a series of preliminary trials, typical composite layups were selected for the joint design assessment and these are shown in Table 2.

Table 2. Layups considered for the joint design assessment.

Layup	Stiffener	Panel
1	16-ply: $[90/45/0/-45]_{2s}$	16-ply: $[90/45/0/-45]_{2s}$
2	16-ply: $[90/45/0/-45]_{2s}$	8-ply: $[90/45/0/-45]_{s}$
3	24-ply: $[90/45/0/-45]_{3s}$	8-ply: $[90/45/0/-45]_{s}$
4	32-ply: $[90/45/0/-45]_{4s}$	8-ply: $[90/45/0/-45]_{s}$
5	16-ply: $[90/45/0/-45]_{2s}$	6-ply: $[0/60/-45]_{s}$
6	16-ply: $[90/45/0/-45]_{2s}$	4-ply: $[90/0]_{s}$
7	16-ply: $[0/45/90/-45]_{2s}$	8-ply: $[0/45/90/-45]_{s}$
8	16-ply: $[45/-45/0/90]_{2s}$	8-ply: $[45/-45/0/90]_{s}$

2.2.2 Design assessment strategy

The adhesive bond layer is usually treated as a potential area of weakness, especially at the bonded overlap end [2, 21, 22]. In the current joint design, the joint strength was dominated by the bond strength and/or the panel condition at the inner bonded overlap end. Hence, the peak stress ratio of the panel/stiffener at the inner bonded overlap end was used to assess the joint design. This stress ratio should be greater than 1 because the stiffener strength is higher than the panel strength. High stress ratio was preferred because it ensured that damage onset and subsequent failure would occur at the inner bonded end. For simplicity, von Mises stress was selected to compute the stress ratio. In addition, the joint design needed to be practical for subsequent manufacturing and testing with limited composite material usage.

3. Finite element modeling and recommendations for the joint design

3.1 Finite element (FE) models

Three-dimensional FE models were created and linear analyses with 2.5 x 2.5 mm 4-node quadrilateral conventional shell elements were conducted via Nastran code. Fig. 4 shows a joint FE model with a series of specific dimensions, in which, a contact pair, stiffener-to-panel, was defined and glued together without the actual adhesive layer. The omission of the actual adhesive layer did not affect the joint design assessment. A tensile displacement, $U_x = 10$ mm combined with $U_y = U_z = 0$, was applied at an independent node that was attached to the nodes within two 25.4 x 50.8 mm bonded-bolted areas at the stiffener side sections via a multi-point constraint (MPC) in RBE2 condition. The left edge of the flat panel was fully fixed with $U_x = U_y = U_z = 0$ displacement boundary conditions (BC).

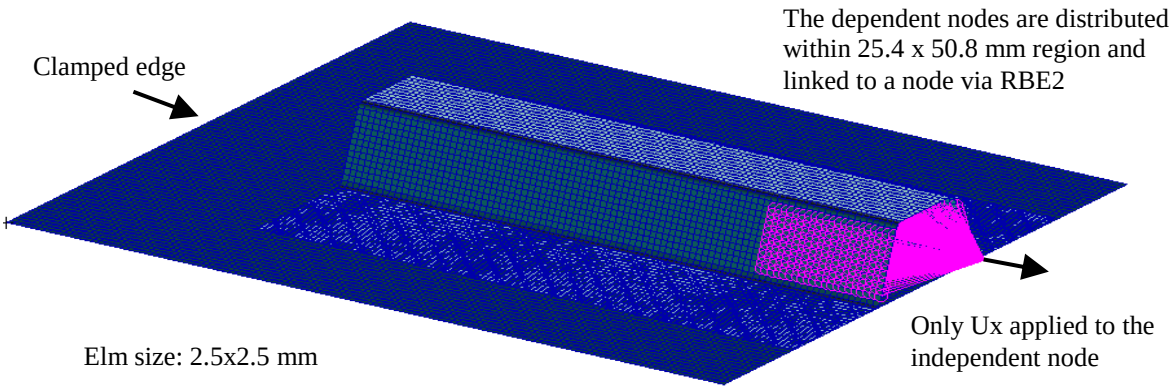

Fig. 4. A 3D FE model for a joint size condition meshed using 4-node quadrilateral conventional shell elements.

3.2 Results and discussion

Variation of peak von Mises stress ratio, panel/stiffener, at the inner bonded overlap end was investigated for the joint design assessment.

3.2.1 Full-field contours in displacement and stress

Secondary bending and stress concentration can be easily identified from full-field variation contours. Fig. 5 shows the full-field contours of deformation and von Mises stress for a specific sized joint in tension. A zero rotation condition at the independent node and the left panel edge was set for the joint in tension and two different layup conditions were displayed. Ignoring the high stresses at the bonded-bolted section, where its strength is much higher than the bonded only region [1, 21], the highly stressed areas were all located at the inner bonded overlap end for the two different layup conditions. The full-field stress contours clearly suggest that the joint strength should be dominated by the strength at the inner bonded overlap end.

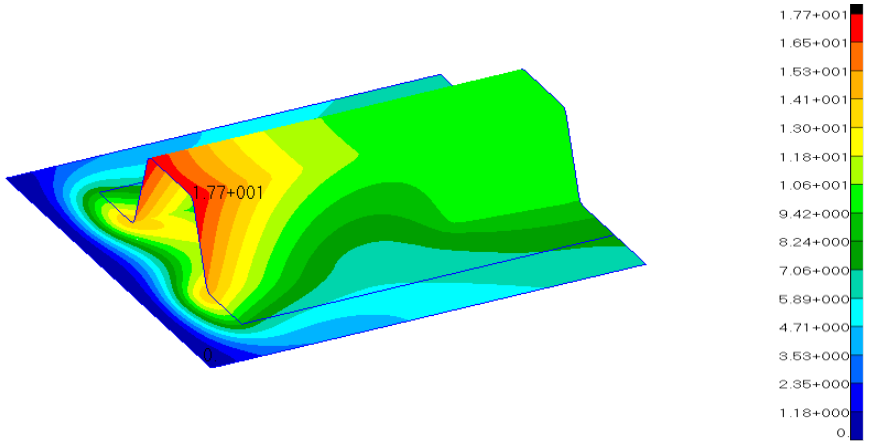

(a) Displacement magnitude (mm) in layup 2 condition

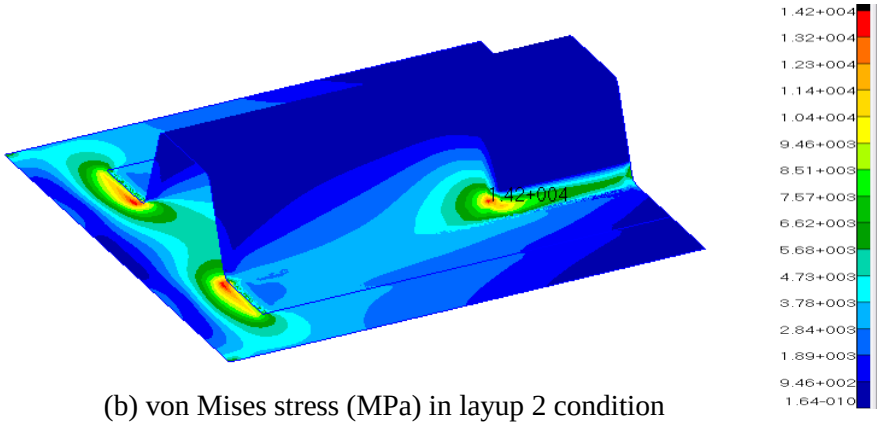

(b) von Mises stress (MPa) in layup 2 condition

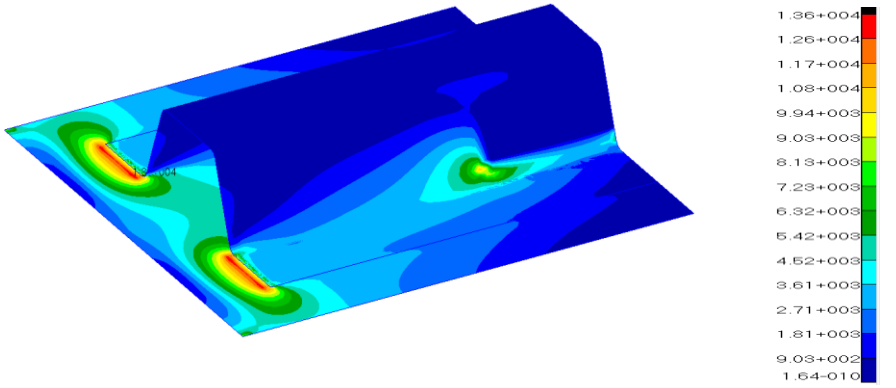

(c) von Mises stress (MPa) in layup 3 condition

Fig. 5. Full-field contours of deformation magnitude (mm) and von Mises stress (MPa) when a specific sized joint was in tension. Where (a) and (b) for the joint with layup 2 condition and (c) for the joint with layup3 condition.

3.2.2 Effects of dimension and layup on the peak stress ratio

A systematic assessment summary of the numerical results is presented in Fig. 6 under zero rotation at the independent node and the panel left edge. Fig. 6(a) shows the peak stress ratio variations, Fig. 6(b) gives the assessed information of the joint dimensional variables, the layup selections, and the resultant stress ratio levels, and Fig. 6(c) presents details of the dimensional variable locations as well as the layup conditions. The results showed that: (i) high values of W1, W2, and L2 resulted in a high stress ratio, while low L1 increased the stress ratio. To ensure success during the joint manufacturing and testing stages, the panel should have certain strength and thickness. Hence, the panel with either 6-ply or 4-ply conditions, as assessed in the layup 5 and 6 conditions, as shown in Fig. 6(b) and (c), were not further considered for the joint design. The highest stress ratio of approximately 2.14 was obtained for the joint with the L2 = 254 mm long stiffener with three different layup selections in 2, 7, and 8. Accordingly, the joint size in assessment 9 (or 14, or 15) combined with the layup condition in 2, 7, or 8 was recommended for the joint design.

3.2.3 Effects of boundary conditions and the L1 level

To considerably eliminate boundary condition (BC) effect on the stress and deformation conditions at the inner overlap end, the L1 level should be higher than the small level of 25.4 mm. Also, having zero rotation at the independent node and the panel left edge being too rigid could not be replicated in the actual loading condition. Therefore, effects of different BCs and L1 levels on the peak stress ratio were studied in this section for the joint with dimensions of W1 = W2 = 25.4 mm and L2 = 254 mm. Comparison of the obtained peak stress ratios is shown in Fig. 7, in which BC1 refers to the boundary conditions with zero rotation at the independent node and the panel left edge, as used in earlier sections 3.2.1 and 3.2.2; BC2 refers to the condition without zero rotation constraint; BC3 refers to the condition with only zero rotation at the panel left end edge; and BC4 refers to the condition with zero rotation at the independent node only. In this assessment, little impact to the peak stress ratio variation was found from the assessed joint layup condition, in 2, 7, or 8. Considerable difference in the peak stress ratio was identified between the two L1 levels under the BC1 condition, which was not shown for other boundary conditions, BC2 to 4. The peak stress ratios were all higher than 1 for the BC2 to BC4 conditions, which suggest that the L1 = 101.6 mm condition would be acceptable for the joint design. As noted, the actual test boundary conditions should be well covered by the BC2 to 4 conditions rather than BC1.

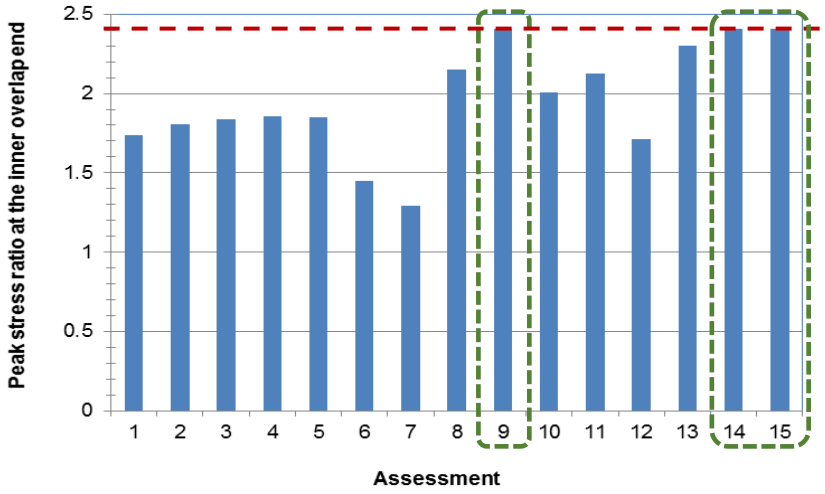

(a)

Assessment	W1	W2	L1	L2	Layup	S-ratio
1	1"	1"	1"	6"	1	1.735099
2	1"	1"	1"	6"	2	1.806656
3	2"	1"	1"	6"	2	1.834711
4	4"	1"	1"	6"	2	1.854975
5	1"	2"	1"	6"	2	1.853088
6	1"	1"	2"	6"	2	1.446721
7	1"	1"	4"	6"	2	1.289398
8	1"	1"	1"	8"	2	2.149362
9	1"	1"	1"	10"	2	2.411067
10	1"	1"	1"	6"	3	2.009646
11	1"	1"	1"	6"	4	2.128
12	1"	1"	1"	6"	5	1.709531
13	1"	1"	1"	6"	6	2.300885
14	1"	1"	1"	10"	7	2.411067
15	1"	1"	1"	10"	8	2.411067

(b)

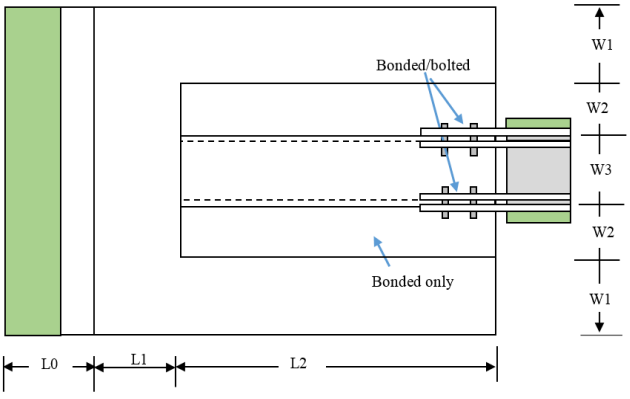

Layup	Stiffener	Panel
1	16-ply: $[90/45/0/-45]_{2s}$	16-ply: $[90/45/0/-45]_{2s}$
2	16-ply: $[90/45/0/-45]_{2s}$	8-ply: $[90/45/0/-45]_{s}$
3	24-ply: $[90/45/0/-45]_{3s}$	8-ply: $[90/45/0/-45]_{s}$
4	32-ply: $[90/45/0/-45]_{4s}$	8-ply: $[90/45/0/-45]_{s}$
5	16-ply: $[90/45/0/-45]_{2s}$	6-ply: $[0/60/-45]_{s}$
6	16-ply: $[90/45/0/-45]_{2s}$	4-ply: $[90/0]_{s}$
7	16-ply: $[0/45/90/-45]_{2s}$	8-ply: $[0/45/90/-45]_{s}$
8	16-ply: $[45/-45/0/90]_{2s}$	8-ply: $[45/-45/0/90]_{s}$

(c)

Fig. 6. Variation of peak (von Mises) stress ratio, panel/stiffener, under influence of layups and dimensions for the joint design assessment, where (a) is the stress ratio variation, (b) are the layup and dimension assessed, and (c) is the information on the layups and the joint dimensions.

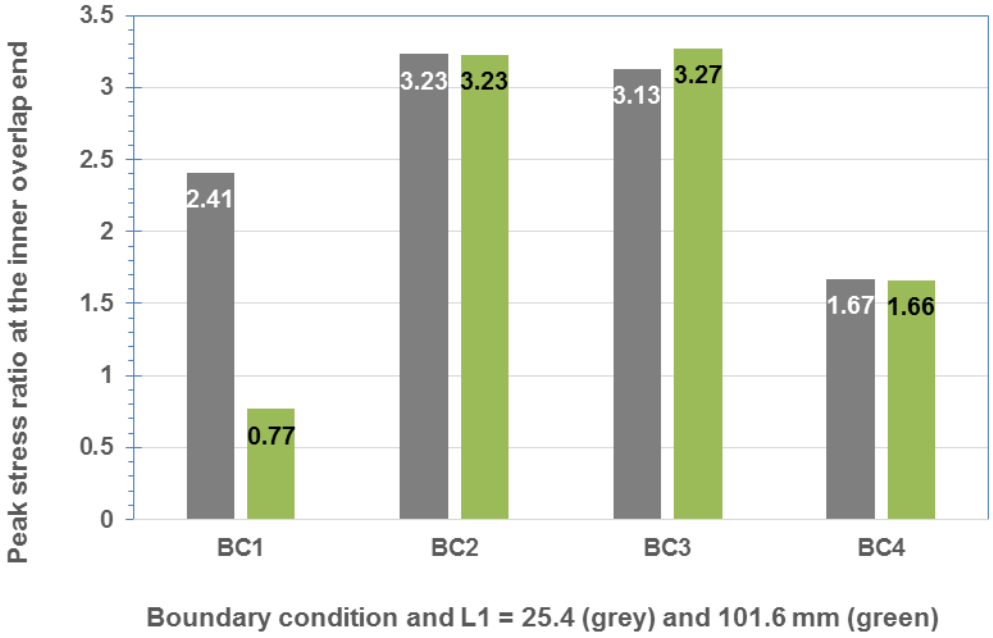

Fig. 7. Variation of peak von Mises stress ratio, panel/stiffener, under the influence of different displacement boundary conditions and the panel unbonded length L1, where the values in grey refer to the L1 = 25.4 mm condition and green refer to the L1 = 101.6 mm condition..

3.3 Recommendations for the joint design

Occurrence of damage onset at the inner overlap end, and the subsequent progressive failure behaviour are expected for the bonded joint due to its tensile load path eccentricity. Therefore, the stress ratio should be an appropriate parameter for the joint design assessment. High stress ratio would meet one of the design requirements that the joint strength be dominated by the condition at the inner overlap end. For practical considerations of the joint design in fabrication, testing, and material usage, the following recommendations were proposed:

(1) Dimensions:

(a) L1 should be long enough, say 101.6 mm or more, to exclude the edge effect on the stress condition at the inner bonded overlap end and make the joint preparation and its subsequent test easier than having a small L1 level;

(b) L2 could be 254 mm long; high L2 level effectively increases the stress ratio; and

(c) W1 and W2 could be as small as 25.4 mm.

(2) Laminate and layups:

(d) The panel should consist of an 8-ply or more plies laminate to ensure a certain thickness and strength for ease of joint fabrication and for testing; while the stiffener should be thicker than the panel, say 2 times the thickness of the panel; and

(e) The layup of $[0/45/90/-45]_{ns}$, $[90/45/0/-45]_{ns}$ (n = 1 for an 8-ply panel and n = 2 for a 16-ply stiffener) should be acceptable for the joint fabrication. The $[0/45/90/-45]_{ns}$ layup condition can effectively reduce the degree of fibre bridging at the bonded interfacial area during testing, as suggested from findings in references [1, 12].

4. Failure load of the designed joint

4.1 Fabricated joint and its 3D FE model

The schematic configuration of a fabricated joint with end fixtures is shown in Fig. 8, in which the layup of the 8-ply panel was $[0/45/90/-45]_s$ and the 16-ply stiffener was $[0/45/90/-45]_{2s}$. The joint dimensions were approximately: L0 = 102 mm, L1 = 120 mm, L2 = 254 mm, W1 = W2 = 25.4 mm. The two pivots, at the two fixture ends for linking grips of a test load frame, were approximately 11.5 mm off the panel mid-plane.

In order to fabricate the steel fixtures with sufficient strength and stiffness, the joint failure load should be known. Also, modelling of the debond and progressive failure behaviour were stage targets within the project scope. Therefore, an advanced 3D FE model meshed with continuum shell elements was developed via Abaqus/CAE, version 6.14r2, as shown in Fig. 9. The 0.15 mm thick adhesive layer was not included in the FE model. The panel and the stiffener were "linked" by contacting each other at the bonded areas using surface-to-surface contact type elements. The panel/stiffener interface interaction, in "node to surface" discretization method, was governed by a cohesive behaviour technique that consisted of a bilinear traction-separation damage law and damage evolution controlled by BK model to model damage onset and evolution at the bonded surface [18-20]. The used parameters in the cohesive behaviour were: (1) stiffness of 5E+8 N/mm3 for the stress conditions in the three modes Knn, Kss, and Ktt; (ii) damage onset with 30 MPa maximum nominal stress for three fracture modes; (iii) damage evolution with the critical strain energy release rate, G_{IC} = 2.8 N/mm for mode 1, and 4 N/mm for the two other shear fracture modes [17-19]. The end steel fixtures were replaced by rigid constraints with "Coupling" type to link the two loading pivots created by using "reference points" in the Abaqus code. Geometrically nonlinear behaviour was set in this numerical investigation. Also, rotation in the out-of-plane at the two loading pivots was not constrained in accordance with the actual testing conditions.

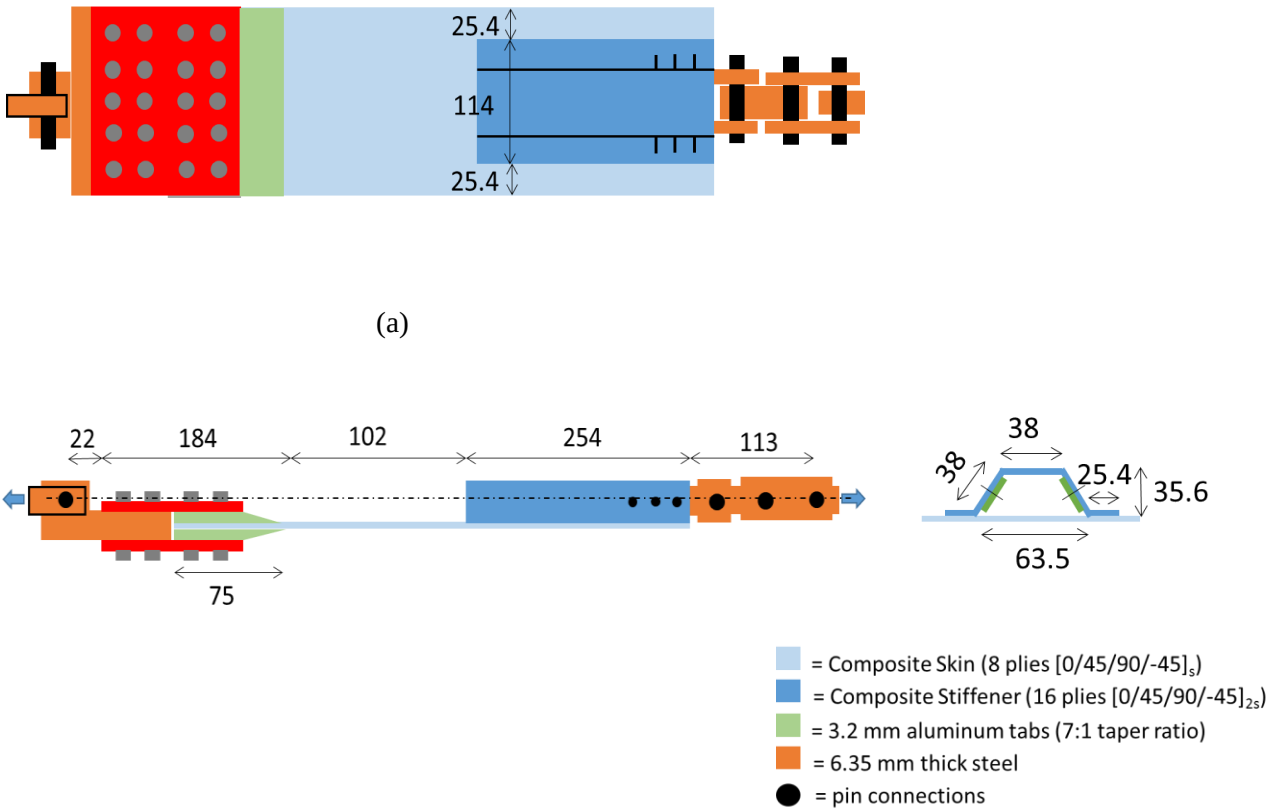

Fig. 8. Schematic configuration of the designed joint with end fixtures (dimensions: mm).

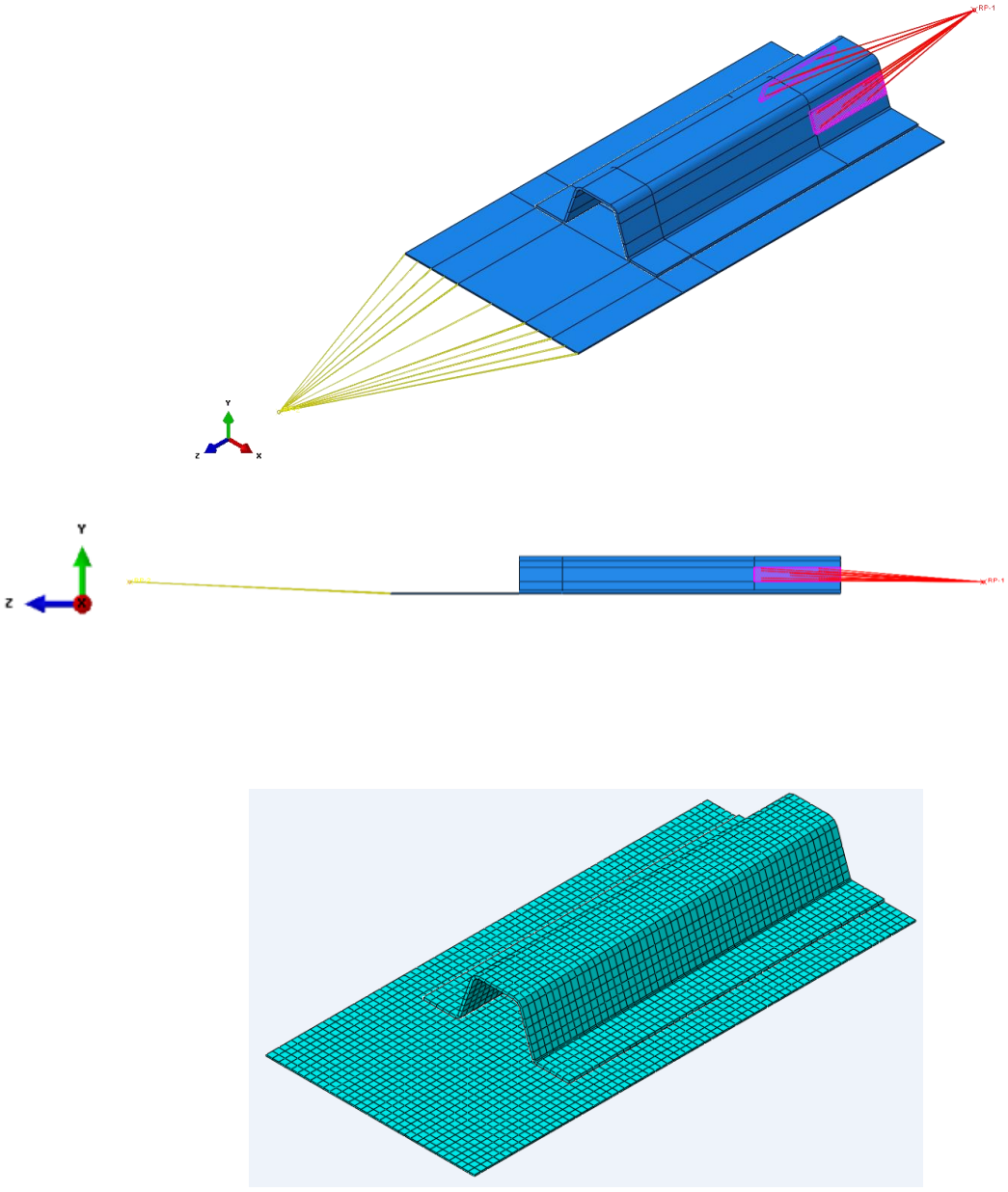

(a)

(b)

(c)

Fig. 9. Three-dimensional finite element using continuous shell elements and cohesive surface behaviour, where (a) and (b) show the rigid attachments for BCs and tensile loading setups, and (c) is for the meshed joint model.

4.2 Failure prediction and correlation with experimental findings

Damage onset and evolution, as well as the resultant progressive failure behaviour, were successfully predicted numerically. Fig. 10 shows debond occurring between the panel and the stiffener initially at the inner overlap end. The predicted failure load was 86.56 kN, which was used as a reference to ensure the proper fixture design and fabrication.

Experimental test was carried out smoothly with the fabricated fixtures; the failure load measured was 86.62 kN. Fig. 11 shows the joint setup and test information. As expected in the numerical modelling, during testing damage started at the inner overlap end and then propagated along the panel/stiffener section until a nearly 90% tensile load drop occurred. Then the joint coupon was removed from the load frame and separated manually. The observed failure modes at the inner overlap end region were: (i) cohesive failure in the adhesive layer, and (ii) fibre peel off and breakage in the panel only.

The fibres peel off and breakages were not covered in the current FE model. Only the major failure mode, cohesive failure, was considered in this FE model. The relative difference between the predicted and the measured failure loads was extremely small, –0.07%. Any discrepancies in the failure load and failure modes between the test and the numerical results should be from the assumed material parameters, model setup, and the pivot off-set level. Excellent agreement in the failure force between the numerical and the experimental results suggest that the parameters used for the damage modelling in the cohesive behaviour technique were very satisfactory.

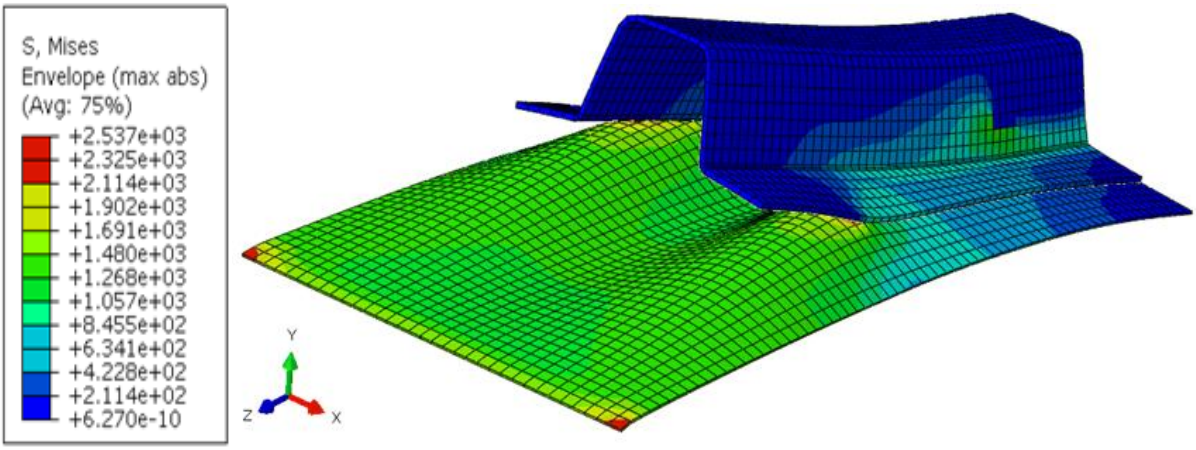

Fig. 10. Predicted failure for the bonded composite joint structure.

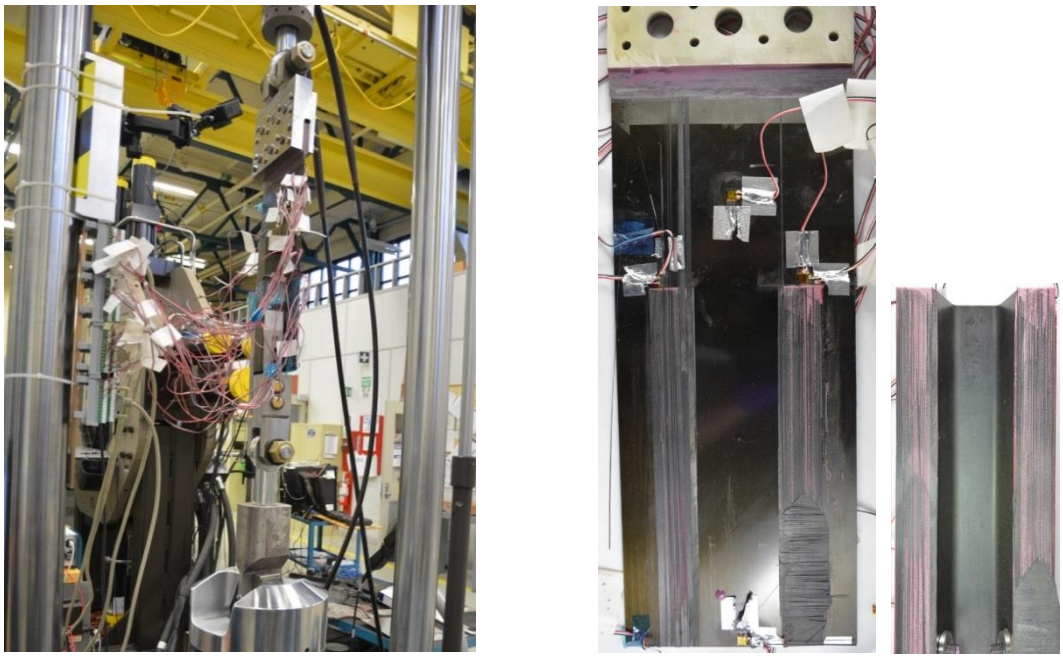

(a) (b)

Fig. 11. Test information of the designed composite joint for: (a) joint setup in a load frame and (b) failure modes of cohesive failure, fibre peel-off and breakage observed on the panel/stiffener interfaces.

5. Concluding remarks

Three-dimensional FE models using conventional shell elements were developed via Nastran code in version 2015r2 for the bonded composite joint design assessment. A parametric study was conducted successfully for the bonded composite joint design based on the peak stress ratio variation at the inner bonded overlap end. The highest stress ratio joint case in the assessment was identified. Consequently, recommendations for dimensions and layups were proposed for the joint design consideration. This effort ensured successful experimental joint design and fabrication.

An advanced 3D FE model using continuum shell elements was developed via Abaqus/CAE code for predicting failure load of the designed joint. With the selected parameters for cohesive behaviour, the model successfully predicted the progressive failure behaviour and joint failure load. Furthermore, the fabricated steel fixtures ensured that the test was completed successfully. The test showed that cohesive failure was one of the major failure modes. Excellent agreement was obtained between the predicted and measured failure load with a relative difference of lea then 1%.

This work provided a good example for using numerical modelling methods to support engineering designs for both test article and testing fixtures. The overall effort provided a sound base for further modelling development to support specific aircraft composite structures damage tolerance and residual strength assessments.

Acknowledgements

Full support from the Department of National Defence (DND), Defence Research and Development Canada (DRDC), and NRC Aerospace Research Centre are acknowledged and greatly appreciated.

References

[1] Li G, Chen JH, Yanishevsky M, and Bellinger NC (2012), Static strength of a composite butt joint configuration with different attachments, *Composite Structures*, 94(5), 1736-1744.

[2] Markatos DN, Tserpes KI, Rau E, Markus S, Ehrhart B, Pantelakis Sp. (2013), The effects of manufacturing-induced and in-service related bonding quality reduction on the mode-I fracture toughness of composite bonded joints for aeronautical use", *Composite Part B*, 45(1), 556–64.

[3] Banea MD, da Silva LFM (2009), Adhesively bonded joints in composite materials: an overview, *Proc inst Mech Eng, Part L: J Mater Des Appl*, 223:1.

[4] Ashtonm HR (1996), Damage Tolerance and durability testing for F/A-18 E/F composite materials structures. In: Proceedings of 37th AIAA/ASME/ASCE/ AHS/ASC structures, structural dynamics & materials conference, Salt Lake City, UT, April, paper AIAA-96-1320-CP; 1996.

[5] Li G, Lee-Sullivan P, and Thring RW (1999), Nonlinear finite element method analysis of stress and strain distributions across the adhesive thickness in composite single-lap joints, *Composite Structures*, 46(4), 395-403.

[6] Li S, Thouless MD, Wass AM, Schroeder JA, Zavattieri PD (2005), Use of mode-I cohesive-zone models to describe the fracture of an adhesively-bonded polymer–matrix composite, *Compos Sci Technol*, 65, 281–93.

[7] Quaresimin M, Ricotta M (2006), Stress intensity factors and strain energy release rates in single lap bonded joints in composite materials. *Compos Sci Technol*, 66, 647–56.

[8] Balzani C, Wagner W, Wilckens D, Degenhardt R, Busing S, Reimerdes HG (2012), Adhesive joints in composite laminates-a combined numerical/experimental estimate of critical energy release rates. *Int J Adhes Adhes*, 32, 23–38.

[9] Bianchi F, Koh TM, Zhang X, Partridge IK, Mouritz AP, (2012), Finite element modelling of z-pinned composite T-joints, *Composite Science and Technology*, 73(1), 48-56.

[10] Li G (2017), Impact modelling of Kevlar fabric composite panels, in proceedings of the 24th Aerospace Structures and Materials Symposium, Canadian Aeronautics and Space Institute, May 16-18, 2017, Toronto, Canada.

[11] Li, G. (2010), Elastic analysis of closed-form solutions for adhesive stresses in bonded single-strap butt joints, *Journal of Mechanics of Materials and Structures*, 5(3), 409-426.

[12] Li, G. (2012), "Theoretical solutions of adhesive stresses in bonded composite butt joints", *Journal of Mechanics of Materials and Structures*, 7(4), 323-346.

[13] Li, G., Johnston, A., Yanishevsky, M., and Bellinger, N.C. (2011), "Elastic deformation analysis of adhesively bonded composite butt joints in tension", *Journal of Aircraft*, 48(2), 578-590.

[14] Williams JG, Hadavinia H (2002), Analytical solutions for cohesive zone models. J. Mech Phys Solids 2002;50(4):809–25.

[15] Zou Z, Reid SR, Li S, Soden PD (2003), Modelling interlaminar and intralaminar damage in filament-wound pipes under quasi-static indentation. *J Compos Mater*, 36(4), 477–99.

[16] Alfano G (2006), On the influence of the shape of the interface law on the application of cohesive-zone models, Compos Sci Technol, 66(6), 723–30.

[17] Li G, Li C (2013), An analytical analysis of energy release rate in bonded composite joints in a mode I condition, *Composites Part B*, 44,704-713.

[18] Li, G. and Li, C. (2014), "Linking bilinear traction law parameters to cohesive zone length for laminated composites and bonded joints", *Advances in Aircraft and Spacecraft Science*, 1(2), 177-196.

[19] Li, G., Li, C. (2015), Assessment of debond simulation and cohesive zone length in a bonded composite joint, *Composites Part B*, 69, 359-368.

[20] Liljedahla CDM, Crocombe AD, Wahaba MA, Ashcroftb IA (2007), Modelling the environmental degradation of adhesively bonded aluminium and composite joints using a CZM approach, *Int J Adhes Adhes*, 27, 505–18.

[21] Li, G. (2013), Fatigue performance characterization of a composite butt joint configuration, *Composites Part A*, 51, 43-55.